Hindawi Publishing Corporation
Journal of Nanotechnology
Volume 2013, Article ID 138457, 10 pages
http://dx.doi.org/10.1155/2013/138457

Research Article

LDPE/HDPE/Clay Nanocomposites: Effects of Compatibilizer on the Structure and Dielectric Response

B. Zazoum, E. David, and A. D. Ngô

Département de Génie Mécanique, École de Technologie Supérieure (ETS), 1100 Notre-Dame Ouest, Montréal, QC, Canada H3C 1K3

Correspondence should be addressed to B. Zazoum; bouchaib.zazoum.1@ens.etsmtl.ca

Received 26 July 2013; Accepted 16 August 2013

Academic Editor: John Zhanhu Guo

PE/clay nanocomposites were prepared by mixing a commercially available premixed polyethylene/O-MMT masterbatch into a polyethylene blend matrix containing 80 wt% low-density polyethylene and 20 wt% high-density polyethylene with and without anhydride modified polyethylene (PE-MA) as the compatibilizer using a corotating twin-screw extruder. In this study, the effect of nanoclay and compatibilizer on the structure and dielectric response of PE/clay nanocomposites has been investigated. The microstructure of PE/clay nanocomposites was characterized using wide-angle X-ray diffraction (WAXD) and a scanning electron microscope (SEM). Thermal properties were examined using differential scanning calorimetry (DSC). The dielectric response of neat PE was compared with that of PE/clay nanocomposite with and without the compatibilizer. The XRD and SEM results showed that the PE/O-MMT nanocomposite with the PE-MA compatibilizer was better dispersed. In the nanocomposite materials, two relaxation modes are detected in the dielectric losses. The first relaxation is due to a Maxwell-Wagner-Sillars interfacial polarization, and the second relaxation can be related to dipolar polarization. A relationship between the degree of dispersion and the relaxation rate f_{max} of Maxwell-Wagner-Sillars was found and discussed.

1. Introduction

There has been growing interest in polymer/nanoclay nanocomposites in recent years because of their outstanding properties at low loading levels as compared with conventional composites. It has been observed that adding small quantities of nanoclay to some thermoplastics as a reinforcing filler to form nanocomposite materials has not only led to more improved mechanical and thermal properties, but also to an enhancement of the dielectric strength and partial discharge resistance [1–10]. However, the understanding of the role of the interfaces of the nanofillers with the molecular mobility mechanism is still rather unsatisfactory.

Although there are different processing methods for preparing nanocomposites, the most widely used technique is the melt-compounding method using a twin-screw extruder, because this technique features economic benefits and ecological advantages. The main challenge in the fabrication of nanocomposites is dispersion of the individual clay platelets into the polymer matrix, due to the incompatibility of hydrophobic matrix with hydrophilic nanoclay [11]. Rendering clay platelets more hydrophobic requires a surface treatment, which is accomplished via ion-exchange reactions with cationic surfactants using quaternary alkyl ammonium cations [12]. For more polar polymers, such as nylon, a surface treatment of layered silicate with an alkyl-ammonium surfactant is sufficient to facilitate exfoliation of the nanofiller within the polymer matrix in some process conditions. However, in the case of polyethylene, it is necessary to use maleic anhydride modified polyethylene PE-g-MA as a compatibilizer to facilitate exfoliation. There are two parameters that contribute to achieving the exfoliation of layered silicates: (1) maleic anhydride content and (2) molecular weight. In general, maleic anhydride modified polyethylene PE-g-MA possesses these two required factors and is widely used as compatibilizer for preparing polyethylene/clay nanocomposites. The most commonly used techniques for evaluating the quality of the dispersion of the nanoclay within the polymer matrix are scanning electron microscopy (SEM), transmission electron microscopy (TEM), and X-ray diffraction (XRD). Only few publications in this field report the use of dielectric methods, which are able to characterize

the level of dispersion and can be combined with microscopic measurements [13–17].

Polyethylene is one of the polyolefins that is used most extensively as ground-wall insulation for medium- to high-voltage applications, and especially for cable insulation, due to its desirable electrical insulating properties, including low relative permittivity ε', low dielectric loss ε'', and high dielectric breakdown strength.

Only a few works have focused on the structure/dielectric response relationship of polyethylene blend nanocomposites. The main objective of this paper is to examine the effect of nanoclay and compatibilizers on the structure and dielectric response of PE/clay nanocomposites prepared by melt-compounding using a corotating twin-screw extruder,and to understand the relationship between these two properties.

2. Experiment

2.1. Materials. The matrix consisted of low-density polyethylene (LDPE, LF-Y819-A, NOVA Chemicals) with a melt flow index (MFI) of 0.75 g/10 min and a density of 0.919 g/cm^3 and high-density polyethylene (HDPE, DGDP-6097 NT 7, DOW) with a melt flow index (MFI) of 10.5 g/10 min and a density of 0.948 g/cm^3. The compatibilizer was anhydride modified polyethylene (PE-MA, E226, Dupont) with a melt flow index (MFI) of 1.75 g/10 min and a density of 0.930 g/cm^3. A commercially available masterbatch of LLDPE/O-MMT (NanoMax) containing 50% organomodified montmorillonite (OMMT) was supplied by Nanocor.

2.2. Preparation of Nanocomposites. The blend of LDPE/HDPE was fixed at a weight ratio of 80/20. The LDPE, HDPE, PEMA, and the commercial masterbatch of LLDPE/O-MMT were dried at 40°C in a vacuum oven for a minimum of 48 hrs prior to extrusion. Nanocomposites were prepared by an extrusion process using a corotating twin-screw extruder (Haake Polylab Rheomex OS PTW16, $D = 16$ mm, $L/D = 40$) coupled with a Haake Metering Feeder to control the feed rate. The temperature profile used in this study was 170–180°C from hopper to die, the feed rate was fixed at 1 kg/hr, and the screw speed was set at 140 rpm. All materials were manually premixed before introduction into the twin-screw extruder. The pellets that were obtained after extrusion were press-molded using an electrically heated hydraulic press to form thin plates (1.2 mm thick). The molding temperature and pressure were 178°C and 5 MPa, respectively. A summary of the compositions of the PE/clay nanocomposites used in this paper is collected in Table 1.

3. Characterization and Measurements

3.1. Differential Scanning Calorimetry (DSC). Thermal parameters (melting temperature, crystallization temperature, and crystallinity) of neat PE, PE/O-MMT, and PE/O-MMT/PE-MA nanocomposites were determined using a Perkin-Elmer DSC Pyris 1 instrument. The calibration of the DSC was performed using indium. All samples had the same weight (approximately 5.0 mg), and the PE and its nanocomposites were heated from 30°C to 180°C during each run at a heating rate of 10°C/min in nitrogen atmosphere. The endothermic and exothermic diagrams were recorded as a function of temperature.

3.2. X-Ray Diffraction (XRD). X-ray diffraction (XRD) was employed in order to assess the degree of dispersion and exfoliation or intercalation state of the nanoclay in the polymer matrix. XRD patterns were identified using a diffractometer (PANalytical X'Pert Pro) with Kα radiation at a wavelength λ of 1.5418 Å and operated at an accelerating voltage of 40 kV and an electrical current of 45 mA. The scanning was conducted from 2° to 9°, with a scan rate of 0.6°/min. The intercalate spacing d_{001} was calculated using Bragg's law:

$$2d \sin\theta = \lambda, \tag{1}$$

where d, θ, and λ represent the interlayer distance of the clay, the measured diffraction angle, and the wavelength, respectively.

3.3. Microscopical Observations. The morphology of the samples was examined using a Hitachi scanning electron microscope (SEM). The samples were first cut in a microtome (Ultraculeika) equipped with a glass knife and then coated with a 2 nm thick layer of platinum in order to avoid electrostatic charging during microscopic observations. The operating voltage was fixed at the lowest possible voltage (5 kV) in order to prevent polymer damage and maintain high-resolution images.

3.4. Dielectric Relaxation Spectroscopy. Dielectric relaxation spectroscopy experiments were carried out using a Novocontrol alpha-N in the 10^{-2} to 10^5 Hz frequency domain at temperatures of 30°, 40°, 50°, 60°, and 70°C. The temperature was controlled using a Novotherm system with a stability of 0.5°C.

Prior to all dielectric spectroscopy measurements, the samples measuring 40 mm in diameter and 1.20 mm in thickness were dried at 50°C in a vacuum oven for 24 hrs and then sandwiched between two gold-plated electrodes measuring 40 mm in diameter to form a parallel-plate geometry capacitor.

The complex dielectric permittivity is given by

$$\varepsilon^*(\omega) = \varepsilon'(\omega) - i\varepsilon''(\omega), \tag{2}$$

where $\varepsilon'(\omega)$ represents the real part, $\varepsilon''(\omega)$ represents the imaginary part, and $\omega = 2\pi f$ represents the angular frequency.

The experimental dielectric data can be fitted into the Havrilialk-Negami equation as shown below:

$$\varepsilon^* = \varepsilon_\infty + \sum_{i=1}^{n} \frac{\Delta\varepsilon_i}{\left(1 + \left(i\omega\tau_i\right)^{\alpha_i}\right)^{\beta_i}}, \tag{3}$$

where ε_∞ represents the high frequency permittivity, $\Delta\varepsilon_i$ represents the ith dielectric relaxation strength, τ_i represents

Table 1: Sample formulation and designation.

Sample designation	LLDPE (wt%)	LDPE/HDPE (wt%)	PE-MA (wt%)	O-MMT (wt%)
MB	50	—	—	50
PE	—	100	0	0
PE/O-MMT	5	90	0	5
PE/O-MMT/PE-MA	5	80	10	5

the relaxation time of the ith relaxation, n represents the number of relaxation processes, and α_i and β_i ($0 < \alpha \leq 1$, $\alpha\beta \leq 1$) represent the shape parameters describing symmetric and asymmetric broadening of the relaxation spectra. At low frequency, the influence of the charge carrier fluctuations must be taken into consideration. The complex permittivity can then be expressed as

$$\varepsilon^* = \varepsilon_\infty + \sum_{i=1}^{n} \left[\frac{\Delta\varepsilon_i}{\left(1 + (i\omega\tau_i)^{\alpha_i}\right)^{\beta_i}} \right] + \frac{\sigma_0}{\varepsilon_0 (i\omega)^s}. \quad (4)$$

By using (2), (3), and (4), the real part $\varepsilon'(\omega)$ and the imaginary part $\varepsilon''(\omega)$ of the complex dielectric permittivity $\varepsilon^*(\omega)$ can be written as

$$\begin{aligned}
\varepsilon'(\omega) &= \varepsilon_\infty + \sum_{i=1}^{n} \left[\Delta\varepsilon_i \cos(\beta_i\varphi_i) \right. \\
&\quad \times \left(\left(1 + 2(\omega\tau_i)^{\alpha_i} \sin\left(\frac{\pi(1-\alpha_i)}{2} \right) \right. \right. \\
&\quad \left. \left. + (\omega\tau)^{2\alpha_i} \right)^{\beta_i/2} \right)^{-1} \Bigg] \\
&\quad + \frac{\sigma_o \omega^{-s}}{\varepsilon_0} \cos\left(\frac{\pi s}{2} \right), \\
\varepsilon''(\omega) &= \sum_{i=1}^{n} \left[\frac{\Delta\varepsilon_i \sin(\beta_i\varphi_i)}{\left(1 + 2(\omega\tau_i)^{\alpha_i} \sin(\pi(1-\alpha_i)/2) + (\omega\tau)^{2\alpha_i} \right)^{\beta_i/2}} \right] \\
&\quad + \frac{\sigma_o \omega^{-s}}{\varepsilon_0} \sin\left(\frac{\pi s}{2} \right),
\end{aligned} \quad (5)$$

where

$$\varphi_i = \tan^{-1}\left[\frac{(\omega\tau_i)^{\alpha_i} \cos(\pi(1-\alpha_i)/2)}{1 + (\omega\tau_i)^{\alpha_i} \sin(\pi(1-\alpha_i)/2)} \right], \quad (6)$$

where σ_o represents dc conductivity and s represents an adjustable parameter. In the case of pure electronic dc conductivity, $s = 1$.

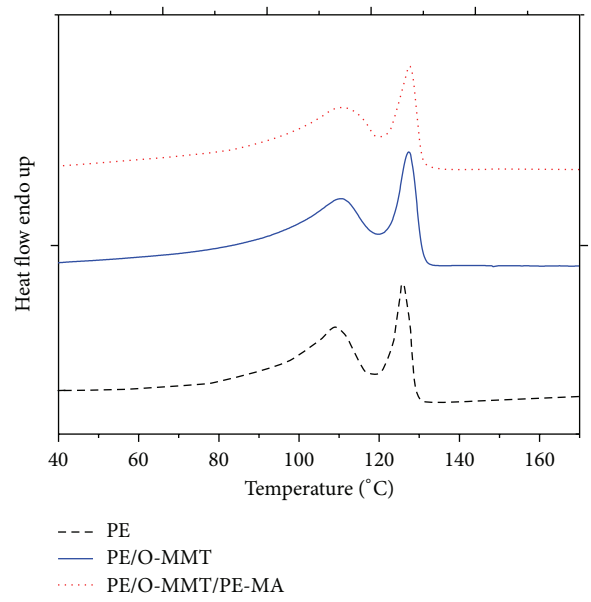

Figure 1: DSC heating thermograms of neat PE, PE/O-MMT, and PE/O-MMT/PE-MA nanocomposites.

4. Results and Discussion

4.1. Thermal Properties. Differential scanning calorimetry (DSC) was used to measure the melting temperatures, crystallization temperatures, and fusion enthalpy ΔH_F. The degree of crystallinity was calculated as expressed by the following equation:

$$\%\chi = \frac{\Delta H_F}{\Delta H_F^0 (1 - \varphi)}, \quad (7)$$

where ΔH_F represents the heat of fusion (J/g), ΔH_F^0 represents the theoretical heat of fusion of 100% crystalline PE (293 J/g), and φ represents the weight fraction of O-MMT in the composites.

The melting and crystallization curves of neat polyethylene and its nanocomposites are depicted in Figures 1 and 2, respectively. The thermal parameters derived from these curves are shown in Table 2. Differential scanning calorimetry (DSC) thermograms revealed two different peak temperatures, with the first melting temperature related to LDPE and the second melting temperature related to HDPE. The melting point peak of LLDPE was not detected due to the low concentration of LLDPE in the nanocomposites. The DSC results clearly showed that the melting temperature,

Table 2: DSC data for PE and its nanocomposites.

Sample	LDPE (T_m, °C)	HDPE (T_m, °C)	LDPE (T_c, °C)	HDPE (T_c, °C)	Heat of fusion of PE (J/g)	Crystallinity of PE (%)
PE	109.4	125.8	97.3	113.5	115.8	39.5
PE/O-MMT	110.6	127.4	97.4	113.4	114.4	41.1
PE/O-MMT/PE-MA	110.9	127.7	98.8	112.7	113.7	40.8

Table 3: 2θ and d_{001} data for the different nanocomposites.

Sample	2θ (°)	d_{001} (nm)
MB	3.13	2.82
PE/O-MMT	2.93	3.02
PE/O-MMT/PEMA	2.72	3.25

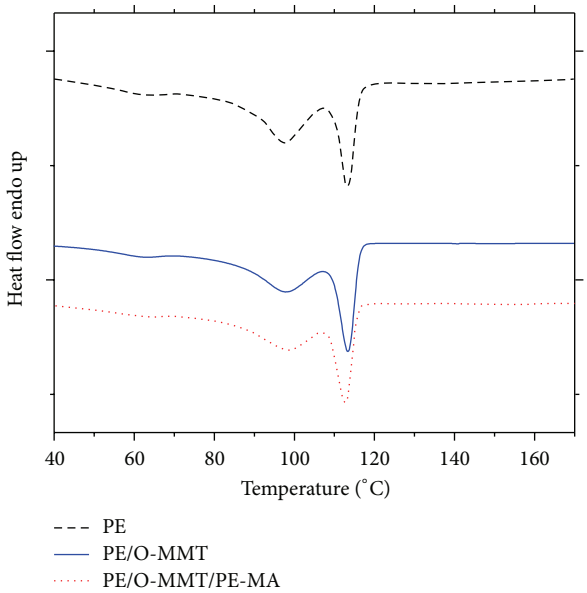

Figure 2: DSC cooling thermograms of neat PE, PE/O-MMT, and PE/O-MMT/PE-MA nanocomposites.

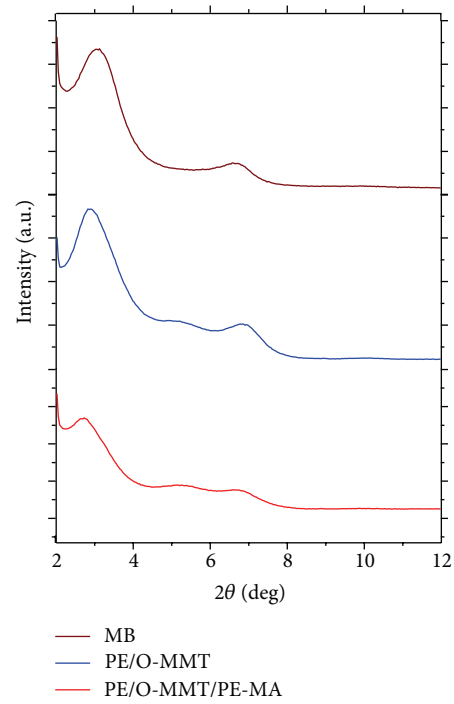

Figure 3: X-ray diffraction patterns for MB and PE nanocomposites with and without compatibilizer.

crystallization temperature, and crystallinity of PE/O-MMT and PE/O-MMT/PE-MA are almost the same as those of neat PE. This behavior suggests that the presence of the organoclay did not create a nucleating effect. The same resultants were found by Morawiec et al. [18].

4.2. Wide-Angle X-Ray Diffraction (WAXD). Figure 3 shows the X-ray diffraction spectra for the O-MMT masterbatch, PE/O-MMT, and PE/O-MMT/PE-MA nanocomposites. The diffraction peak for the O-MMT masterbatch is approximately $2\theta = 3.13°$, which corresponds to a d_{001} value of 2.82 nm calculated using the Bragg law (Table 3). When the O-MMT masterbatch was diluted with pure PE to create PE/O-MMT nanocomposites, the diffraction peak was found to shift to a smaller angle of 2.93°, indicating the increase in d_{001} spacing of the galleries of the organoclay. This improvement in the dispersion was due to the processing conditions for the fabrication of nanocomposites. For the ternary nanocomposites PE/O-MMT/PE-MA, the diffraction peak was observed at a lower angle of 2.73°, corresponding to an increase in intercalate spacing d_{001} to 3.25 nm. On the other hand, the reduction in the diffraction intensity accompanied by the broadening of the basal peak in the PE/O-MMT/PE-MA nanocomposites suggests that the degree of dispersion of the nanoclay within the polymer matrix was improved and that these compatibilized nanocomposites contain a significant proportion of exfoliated nanoclay in the final nanocomposites. This is due to the polar interactions between the maleic anhydride groups in the PE-MA and the OH groups of clay which lead to a formation of a covalent bond between clay and compatibilizer and help polymer chains to penetrate the galleries of the organoclay easily [6, 19, 20]. Since PE-MA has a high molecular weight (low melt index), the shear stress was significant, which led to an increase in the delamination of the clay platelets [1, 21–27].

4.3. Morphological Characterizations by SEM. In order to confirm the XRD results, the morphology of the nanocomposites was observed using a scanning electronic microscopy

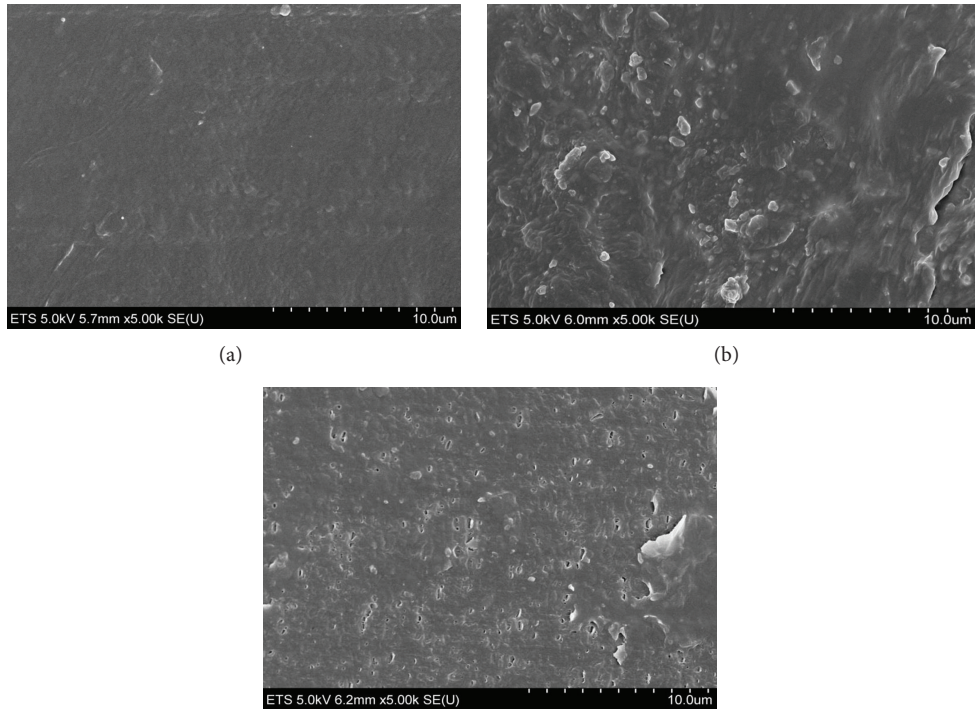

Figure 4: Representative SEM micrographs for (a) neat PE, (b) PE/O-MMT, and (c) PE/OMMT/PE-MA.

(SEM). Figure 4 shows the morphology of neat PE (Figure 4(a)), PE/O-MMT (Figure 4(b)), and the ternary nanocomposites PE/O-MMT/PE-MA (Figure 4(c)) at a magnification of 5,000. For PE/O-MMT nanocomposites, the existence of the clay aggregates or tactoids can be seen at the micrometer level, and therefore, the morphology is not homogeneous, which reveals a poor intercalated/exfoliated structure. However, when the compatibilizer was added, it was observed that the density and size of the aggregates decreased, which indicates that the dispersion of nanoclays within the polymer matrix is much better. This is consistent with the higher intercalate spacing d_{001} and the reduction in the diffraction intensity accompanied by the broadening of the peak observed in the XRD results (Figure 3 and Table 3).

4.4. Broadband Dielectric Spectroscopy. Polyethylene is classified as a nonpolar polymer with low dielectric permittivity. In general, this type of material exhibits no notable or significant ionic, interfacial, or dipolar polarization, being characterized by low flat dielectric losses. As observed from Figure 5(a), the relative permittivity (ε') of neat PE remains essentially constant in the 10^{-2} to 10^{5} frequency range, showing a small decrease when the temperature is increased. The slight decrease in (ε') at higher temperatures can be related to a combination of water evaporation and a decrease in the density [17]. However, the dielectric loss (ε'') of neat PE at low frequency (Figure 5(b)) shows a significant increase, which can be attributed to the contribution of charge carriers leading to various forms of conductivity and electrode polarization [28]. This is the so-called low-frequency dispersion. As expected, no relaxation process is detected in this material.

For PE/O-MMT nanocomposites, Figure 6 shows the frequency dependence of relative permittivity ε' and dielectric loss ε'' at various temperatures. It can be seen that the relative permittivity ε' shows two sharp decreases (Figure 6(a)), corresponding to the two peaks in the dielectric losses ε'' (Figure 6(b)). This indicates that the nanocomposites exhibited two dielectric relaxation processes. It is evident that the ε'' peaks observed in PE/OMMT nanocomposites are due to the addition of nanoclay, because no dielectric relaxations were observed for the neat PE. The peaks of the relaxation processes presented in the nanocomposites were shifted to higher frequencies as the temperature was increased. This change shows that the relaxation processes exhibited thermal activation behaviour.

In order to clearly show the relaxation processes observed in PE/O-MMT nanocomposites, the dielectric loss (ε'') was plotted as a function of the frequency and temperature in a 3D representation (Figure 7). Two relaxation modes were observed in the dielectric losses. The first relaxation was detected at low frequency, and it is attributable to a Maxwell-Wagner-Sillars polarization associated with the blocking of charges at the interfaces between two inhomogeneous phases with different conductivity, such as the polymer matrix and the silicates filler [29–31]. The second relaxation, which was detected at high frequency, can be attributed to dipolar polarization associated with the polar characteristic of the intercalant that was used for surface treatment of

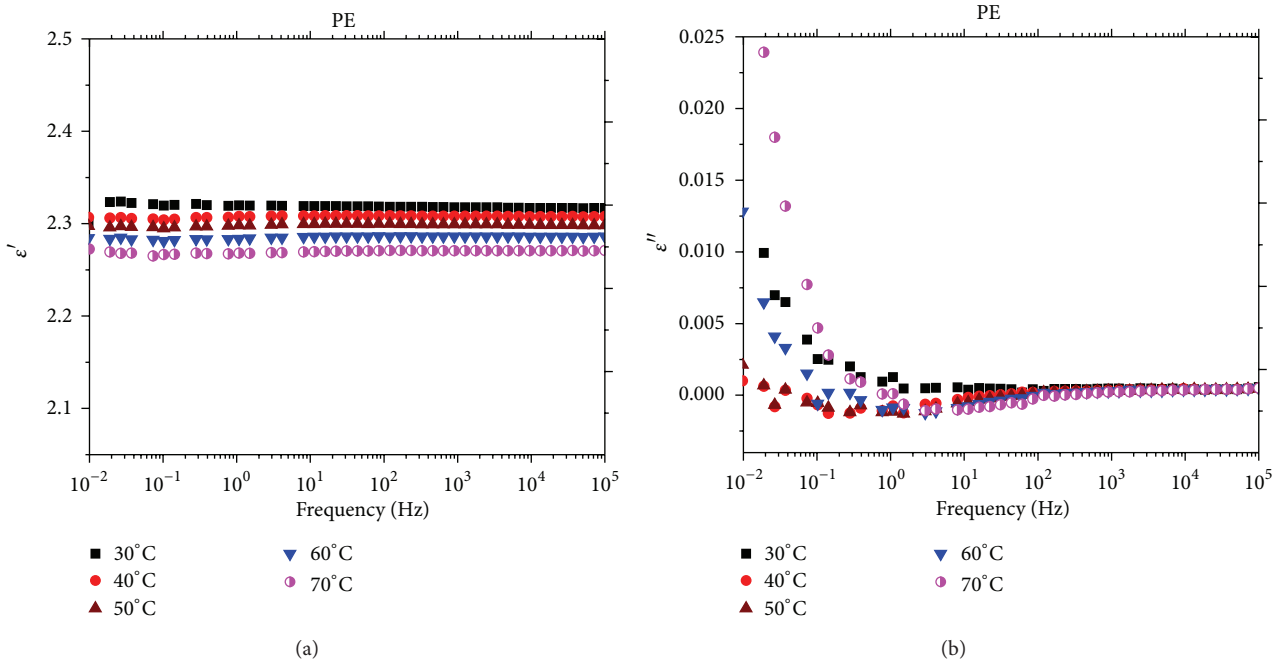

Figure 5: Relative permittivity ε' (a) and dielectric loss ε'' (b) versus frequency at various temperatures observed for the neat PE blend.

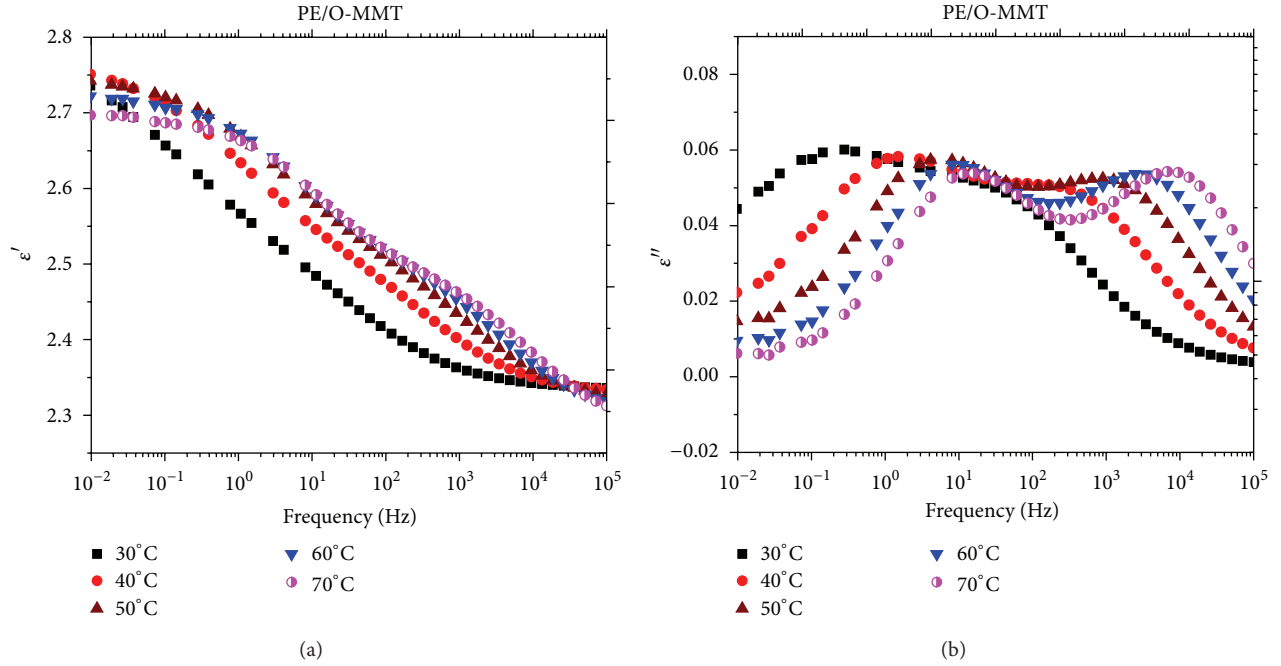

Figure 6: Relative permittivity ε' (a) and dielectric loss ε'' (b) for PE/O-MMT nanocomposites versus frequency at different temperatures.

montmorillonite clay in order to improve compatibility and dispersion of the hydrophilic clay within the hydrophobic polymer matrix.

The experimental data related to the dielectric loss ε'' for PE/O-MMT nanocomposites were fitted into the Havrilialk-Negami function (Figure 8), and the optimum dielectric parameters are shown in Table 4.

Figure 9 shows the frequency dependence of the permittivity ε' (Figure 9(a)) and the dielectric loss ε'' (Figure 9(b)) for PE/O-MMT/PE-MA. As observed for PE/O-MMT, the two relaxation processes are also presented for these compatibilized nanocomposites. It can be seen that the relaxation peaks are more thermally activated in PE/O-MMT/PE-MA than in PE/O-MMT.

In order to study the temperature dependence of both relaxation processes for the PE/O-MMT nanocomposites, the relaxation rate f_{max} of the Maxwell-Wagner-Sillars and dipolar polarization processes were plotted versus inverse

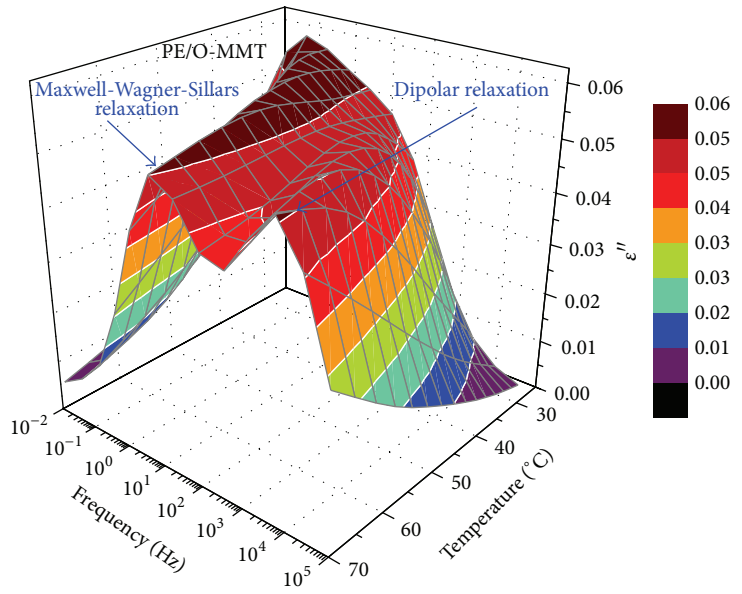

Figure 7: Dielectric loss (ε'') for PE/O-MMT nanocomposites versus frequency at various temperatures, plotted in 3D representation.

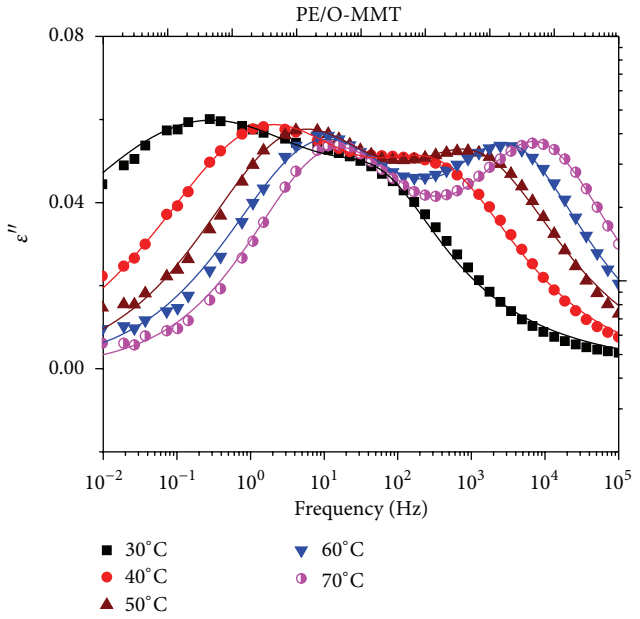

Figure 8: Dielectric loss ε'' for PE/O-MMT nanocomposites versus frequency at different temperatures with the optimum fitting curves for the Havrilialk-Negami equation.

Table 4: Optimum fit parameters for MWS and dipolar relaxations in Figure 8.

(a)

	MWS polarization			
T (°C)	α_1	β_1	$\Delta\varepsilon_1$	τ_1 (s)
30	0.29	1.00	0.50	0.56
40	0.43	1.00	0.32	0.11
50	0.48	1.00	0.27	0.04
60	0.49	0.98	0.26	0.02
70	0.55	0.89	0.23	0.01

(b)

	Dipolar polarization			
T (°C)	α_2	β_2	$\Delta\varepsilon_2$	τ_2 (s)
30	0.79	0.87	0.05	$260E-5$
40	0.67	0.63	0.14	$60.8E-5$
50	0.62	0.70	0.18	$17.7E-5$
60	0.67	0.68	0.18	$6.45E-5$
70	0.63	0.81	0.19	$2.35E-5$

temperatures, as shown in Figure 10. The data were found to be in agreement with the Arrhenius equation:

$$f_{\max}(T) = f_{\infty} \exp\left(-\frac{E_A}{k_\beta T}\right), \quad (8)$$

where f_{∞} represents the preexponential factor, E_A represents the activation energy, and k_β represents the Boltzmann constant. It can be seen that both processes follow Arrhenius' law, with activation energies of 1.2 eV and 1.6 eV for the Maxwell-Wagner-Sillars and dipolar relaxation, respectively.

It is evident from Figure 11 that the values of the relaxation rate $f_{\max}$ of Maxwell-Wagner-Sillars are significantly influenced by the structure of the nanocomposites, with the values of $f_{\max}$ being higher in the well-dispersed PE/O-MMT/PE-MA nanocomposites than in the PE/O-MMT nanocomposites. In order to better understand the relationship between the structure and the relaxation rate $f_{\max}$ of the Maxwell-Wagner-Sillars relaxation process, Böhning et al. [14] suggest

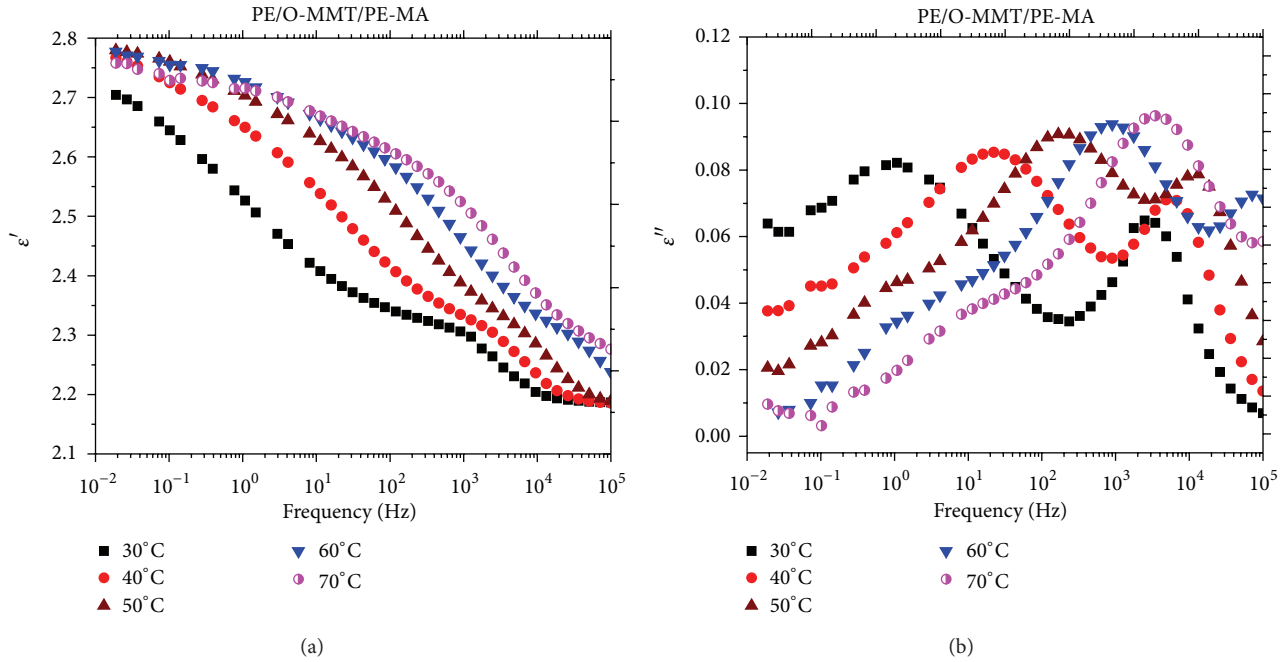

FIGURE 9: Relative permittivity ε' (a) and dielectric loss ε'' (b) for PE/O-MMT/PE-MA nanocomposites versus frequency at different temperatures.

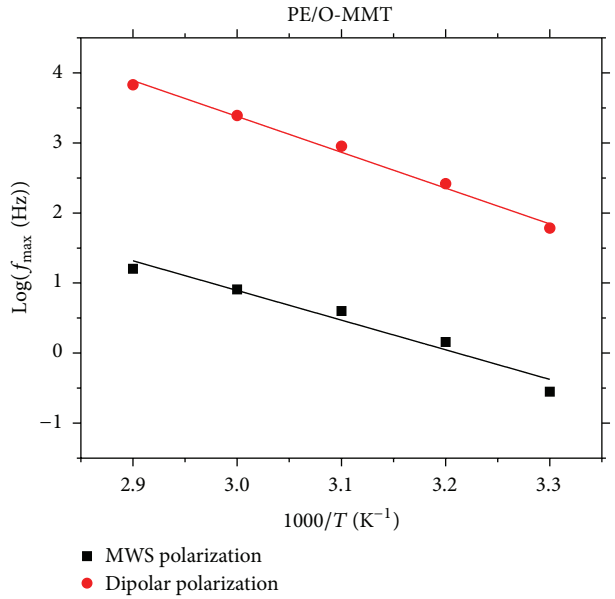

FIGURE 10: Relaxation rate f_{max} as a function of inverse temperature for the two relaxation modes observed in PE/O-MMT nanocomposites. The solid lines represent best fits for the Arrhenius function.

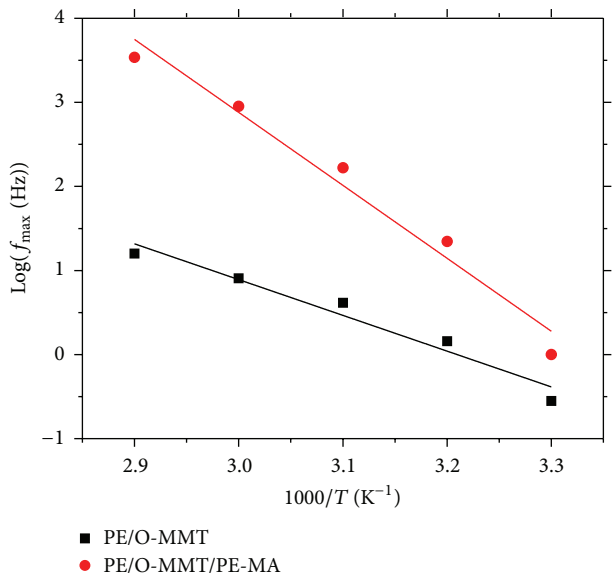

FIGURE 11: Relaxation rate f_{max} as a function of inverse temperature for the MWS relaxation rate observed in PE/O-MMT and PE/O-MMT/PE-MA nanocomposites. The solid lines represent best fits for the Arrhenius function.

that f_{max} is inversely proportional to the mean distance d between separated nanoclay layers:

$$\frac{f_{max\,2}}{d_1} \approx \frac{f_{max\,1}}{d_2}. \quad (9)$$

Accordingly, the improvement in the degree of dispersion in PE/O-MMT/PE-MA nanocomposites obtained with the addition of the compatibilizer leads to a decrease in the mean distance between the clay layers and consequently an increase in the relaxation rate f_{max} for the Maxwell-Wagner- Sillars process.

5. Conclusion

A commercially available premixed polyethylene/O-MMT masterbatch was used in this study to prepare PE/O-MMT nanocomposites using a corotating twin-screw extruder.

The quality of dispersion was improved by the incorporation of anhydride modified polyethylene (PE-MA) as the compatibilizer. This is due to the fact that PE-MA helps polymer chains to penetrate the galleries of the organoclay easily. No relaxation processes were observed in the neat PE, but two thermally activated relaxation modes were observed in the nanocomposite materials: a low-frequency relaxation that can be attributed to an interfacial process and a high-frequency relaxation that is related to a dipolar polarization process. It was observed that the relaxation rate of the Maxwell-Wagner-Sillars process increased as the degree of dispersion increased. This correlation shows that broadband dielectric spectroscopy can be used as a macroscopic tool to evaluate the quality of dispersion in nanocomposite materials.

Conflict of Interests

The authors declare that there is no conflict of interests regarding the publication of this paper.

Acknowledgment

The authors are grateful for the financial support revived from the National Sciences and Engineering Research Council of Canada (NSERC).

References

[1] M. Kawasumi, N. Hasegawa, M. Kato, A. Usuki, and A. Okada, "Preparation and mechanical properties of polypropylene-clay hybrids," *Macromolecules*, vol. 30, no. 20, pp. 6333–6338, 1997.

[2] H. Tan and W. Yang, "Toughening mechanisms of nanocomposite ceramics," *Mechanics of Materials*, vol. 30, no. 2, pp. 111–123, 1998.

[3] Y. Han, Z. Wang, X. Li, J. Fu, and Z. Cheng, "Polymer-layered silicate nanocomposites: synthesis, characterization, properties and applications," *Current Trends in Polymer Science*, vol. 6, pp. 1–16, 2001.

[4] X. Kornmann, H. Lindberg, and L. A. Berglund, "Synthesis of epoxy-clay nanocomposites: influence of the nature of the clay on structure," *Polymer*, vol. 42, no. 4, pp. 1303–1310, 2001.

[5] L. A. Utracki and M. R. Kamal, "Clay-containing polymeric nanocomposites," *Arabian Journal for Science and Engineering*, vol. 27, no. 1, pp. 43–67, 2002.

[6] S. Hotta and D. R. Paul, "Nanocomposites formed from linear low density polyethylene and organoclays," *Polymer*, vol. 45, no. 22, pp. 7639–7654, 2004.

[7] K. Zhao and K. He, "Dielectric relaxation of suspensions of nanoscale particles surrounded by a thick electric double layer," *Physical Review B*, vol. 74, no. 20, Article ID 205319, 10 pages, 2006.

[8] H. Awaji, Y. Nishimura, S. Choi, Y. Takahashi, T. Goto, and S. Hashimoto, "Toughening mechanism and frontal process zone size of ceramics," *Journal of the Ceramic Society of Japan*, vol. 117, no. 1365, pp. 623–629, 2009.

[9] L. Chen and G. Chen, "Relaxation behavior study of silicone rubber crosslinked network under static and dynamic compression by electric response," *Polymer Composites*, vol. 30, no. 1, pp. 101–106, 2009.

[10] P. Kim, N. M. Doss, J. P. Tillotson et al., "High energy density nanocomposites based on surface-modified $BaTiO_3$ and a ferroelectric polymer," *ACS Nano*, vol. 3, no. 9, pp. 2581–2592, 2009.

[11] M. A. Osman, J. E. P. Rupp, and U. W. Suter, "Tensile properties of polyethylene-layered silicate nanocomposites," *Polymer*, vol. 46, no. 5, pp. 1653–1660, 2005.

[12] X. Zhang, Z. Liu, Q. Li, Y. Leung, K. Ip, and S. Hark, "Routes to grow well-aligned arrays of ZnSe nanowires and nanorods," *Advanced Materials*, vol. 17, no. 11, pp. 1405–1410, 2005.

[13] R. D. Davis, A. J. Bur, M. McBrearty, Y. Lee, J. W. Gilman, and P. R. Start, "Dielectric spectroscopy during extrusion processing of polymer nanocomposites: a high throughput processing/characterization method to measure layered silicate content and exfoliation," *Polymer*, vol. 45, no. 19, pp. 6487–6493, 2004.

[14] M. Böhning, H. Goering, A. Fritz et al., "Dielectric study of molecular mobility in poly(propylene-graft-maleic anhydride)/clay nanocomposites," *Macromolecules*, vol. 38, no. 7, pp. 2764–2774, 2005.

[15] N. Noda, Y. H. Lee, A. J. Bur et al., "Dielectric properties of nylon 6/clay nanocomposites from on-line process monitoring and off-line measurements," *Polymer*, vol. 46, no. 18, pp. 7201–7217, 2005.

[16] P. J. Purohit, J. E. Huacuja-Sánchez, D. Wang et al., "Structure-property relationships of nanocomposites based on polypropylene and layered double hydroxides," *Macromolecules*, vol. 44, no. 11, pp. 4342–4354, 2011.

[17] V. Tomer, G. Polizos, C. A. Randall, and E. Manias, "Polyethylene nanocomposite dielectrics: implications of nanofiller orientation on high field properties and energy storage," *Journal of Applied Physics*, vol. 109, no. 7, Article ID 074113, 11 pages, 2011.

[18] J. Morawiec, A. Pawlak, M. Slouf, A. Galeski, E. Piorkowska, and N. Krasnikowa, "Preparation and properties of compatibilized LDPE/organo-modified montmorillonite nanocomposites," *European Polymer Journal*, vol. 41, no. 5, pp. 1115–1122, 2005.

[19] T. G. Gopakumar, J. A. Lee, M. Kontopoulou, and J. S. Parent, "Influence of clay exfoliation on the physical properties of montmorillonite/polyethylene composites," *Polymer*, vol. 43, no. 20, pp. 5483–5491, 2002.

[20] M. J. Dumont, A. Reyna-Valencia, J. P. Emond, and M. Bousmina, "Barrier properties of polypropylene/organoclay nanocomposites," *Journal of Applied Polymer Science*, vol. 103, no. 1, pp. 618–625, 2007.

[21] N. Hasegawa, M. Kawasumi, M. Kato, A. Usuki, and A. Okada, "Preparation and mechanical properties of polypropylene-clay hybrids using a maleic anhydride-modified polypropylene oligomer," *Journal of Applied Polymer Science*, vol. 67, no. 1, pp. 87–92, 1998.

[22] N. Hasegawa, H. Okamoto, M. Kato, and A. Usuki, "Preparation and mechanical properties of polypropylene-clay hybrids based on modified polypropylene and organophilic clay," *Journal of Applied Polymer Science*, vol. 78, no. 11, pp. 1918–1922, 2000.

[23] M. Kato, A. Usuki, and A. Okada, "Synthesis of polypropylene oligomer-clay intercalation compounds," *Journal of Applied Polymer Science*, vol. 66, no. 9, pp. 1781–1785, 1997.

[24] P. Maiti, P. H. Nam, M. Okamoto, N. Hasegawa, and A. Usuki, "Influence of crystallization on intercalation, morphology, and mechanical properties of polypropylene/clay nanocomposites," *Macromolecules*, vol. 35, no. 6, pp. 2042–2049, 2002.

[25] E. Manias, A. Touny, L. Wu, K. Strawhecker, B. Lu, and T. C. Chung, "Polypropylene/montmorillonite nanocomposites. Review of the synthetic routes and materials properties," *Chemistry of Materials*, vol. 13, no. 10, pp. 3516–3523, 2001.

[26] P. H. Nam, P. Maiti, M. Okamoto, T. Kotaka, N. Hasegawa, and A. Usuki, "A hierarchical structure and properties of intercalated polypropylene/clay nanocomposites," *Polymer*, vol. 42, no. 23, pp. 9633–9640, 2001.

[27] Y. Wang, F. B. Chen, K. C. Wu, and J. C. Wang, "Shear rheology and melt compounding of compatibilized-polypropylene nanocomposites: effect of compatibilizer molecular weight," *Polymer Engineering and Science*, vol. 46, no. 3, pp. 289–302, 2006.

[28] F. Kremer and A. Schönhals, *Broadband Dielectric Spectroscopy*, Springer, New York, NY, USA, 2003.

[29] E. Laredo, M. Grimau, F. Sánchez, and A. Bello, "Water absorption effect on the dynamic properties of nylon-6 by dielectric spectroscopy," *Macromolecules*, vol. 36, no. 26, pp. 9840–9850, 2003.

[30] H. M. Le Huy and J. Rault, "Remarks on the α and β transitions in swollen polyamides," *Polymer*, vol. 35, no. 1, pp. 136–139, 1994.

[31] D. W. McCall and E. W. Anderson, "Dielectric properties of linear polyamides," *The Journal of Chemical Physics*, vol. 32, no. 1, pp. 237–241, 1960.